Emulation of an OWC Ocean Energy Plant With PMSG and Irregular Wave Model

Dionisio Ramirez, *Senior Member, IEEE*, Juan Pablo Bartolome, Sergio Martinez, *Member, IEEE*, Luis Carlos Herrero, *Member, IEEE*, and Marcos Blanco

***Abstract*—Ocean energy is a promising resource for renewable electricity generation that presents many advantages, such as being more predictable than wind energy, but also some disadvantages such as large and slow amplitude variations in the generated power. This paper presents a hardware-in-the-loop prototype that allows the study of the electric power profile generated by a wave power plant based on the oscillating water column (OWC) principle. In particular, it facilitates the development of new solutions to improve the intermittent profile of the power fed into the grid or the test of the OWC behavior when facing a voltage dip. Also, to obtain a more realistic model behavior, statistical models of real waves have been implemented.**

***Index Terms*—Oscillating water column (OWC), renewable energy, ride through, wave energy.**

I. Introduction

OCEAN ENERGY is a promising source for electricity generation. Although there are hundreds of descriptions of wave energy conversion systems available in the literature [1], there are only a few prototypes deployed in real sea conditions. Among them, the systems closest to industrial exploitation are those based on the oscillating water column (OWC) principle [2]–[4] (Fig. 1). The pressure exerted by the wave on the air inside a chamber generates an air flow that drives an air turbine. As the water level inside the chamber increases, it pushes the air in the chamber through a turbine driving an electric generator. When the water level decreases, air is sucked into the chamber and now goes in the opposite direction through the turbine. Despite the alternating air flow, most of the power take off (PTO) systems used with OWC devices maintain a continuous rotation direction, for instance, using a Wells turbine.

Several experimental facilities have functioned for years [2], and recently, a commercial power plant has been inaugurated in a breakwater in Mutriku, Spain, with 16 chambers and turbines, with a total installed power of 296 kW, and an estimated annual production of 600 000 kWh.

Manuscript received February 20, 2015; revised May 26, 2015; accepted July 07, 2015. Date of publication August 04, 2015; date of current version September 16, 2015. This work was supported in part by the Spanish Ministry of Economy and Competitivity under Grant ENE2012-36981. Paper no. TSTE-00128-2015.

D. Ramirez, J. P. Bartolome, S. Martinez, and M. Blanco are with the Department of Electrical Engineering, ETSI Industriales, Technical University of Madrid, Madrid 28006, Spain (e-mail: dionisio.ramirez@upm.es).

L. C. Herrero is with the Department of Electronics Technology, University of Valladolid, Valladolid 47014, Spain.

Color versions of one or more of the figures in this paper are available online at http://ieeexplore.ieee.org.

Digital Object Identifier 10.1109/TSTE.2015.2455333

From the point of view of the electric grid to which they are connected, and similar to other renewable energy technologies [5], most of the generation systems based on wave energy have a common problem: the power fed into the grid has large and slow amplitude variations, which are difficult to filter [6], [7].

This paper presents a system developed in our university to investigate possible solutions to this problem. Previously described systems are based on the use of pure sinusoidal wave profiles [8]. However, there is a need to emulate a behavior closer to reality. The developed system incorporates the possibility to emulate irregular waves using statistical models that reproduce real waves recorded in certain areas of the ocean by measuring buoys.

Each of the models that can be reproduced with the system represents waves in a different type of sea [8]. The type of system modeled in this prototype is an onshore OWC, either with deep water or with finite water depth.

The developed prototype is a hardware-in-the-loop system in which the hardware part is the electrical generation subsystem. The rest of the plant, from the incident wave to the turbine shaft, is mathematically modeled. Section II describes these simulation models and Section III describes the hardware part of the prototype. Section IV shows the developed interfaces used to configure the system and, finally, Section V presents some experimental results obtained in the tests, showing the performance and capabilities of the prototype, and a relevant application in electrical engineering research for testing the fault-ride-through capability of the emulated OWC plant.

II. Implemented Models

As the main objective of the prototype is to be used to test new electrical solutions to the problems related to the grid connection of this kind of power plants (e.g., the large and slow fluctuations in the generated electric power) and, as from this point of view, high accurate hydrodynamic and mechanical models are not necessary, simplified models of wave spectrums, chamber, and turbine have been adopted.

A. Irregular Wave Model

In this model, the state of the free surface of the sea is represented by its frequency spectrum $S(\omega)$. For real waves, this spectrum is calculated from measurements obtained with oceanographic buoys and it gives information about the energy content for the different frequencies into which the real wave can be decomposed. Also, $S(\omega)$ allows to reproduce in the time

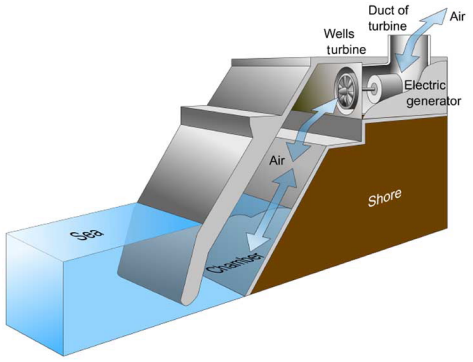

Fig. 1. Schematic representation of an OWC power plant.

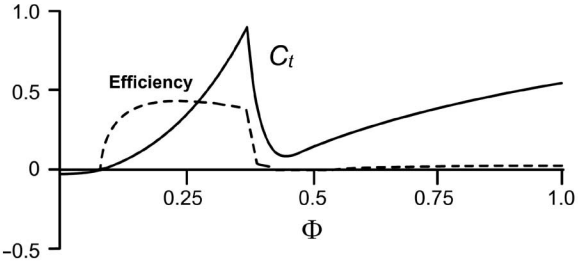

Fig. 2. Generic C_t and efficiency as a function of the flow coefficient, used to model the Wells turbine. The profiles can be easily configured using a user interface. The graph is symmetrical with respect to the y-axis for negative values of Φ.

domain, a sea state with the same spectral characteristics (peak period, significant height, etc.) as the original measured real waves.

Also, the spectrum of a wave may be mathematically defined from empirical equations obtained from the observation of sea properties. The developed prototype implements three different spectrums to describe the sea state incident to the OWC: Pierson–Moskowitz [8]–[11], JONSWAP [12]–[15], TMA [8], [16], and Bretschneider [17].

The related equations make information management easier and can characterize a sea state using a few parameters. Nevertheless, to build the irregular wave profile from the frequency spectrum, it is necessary to calculate and to add a large number of sinusoidal terms. However, the higher the number of harmonics is, the longer the processing time is. Moreover, as the calculation is carried out in real time by a microprocessor, in which the control of the OWC prototype is implemented, the number of harmonics that can be represented will be low. For this reason, the offline calculation in a PC of the wave profile from the wave spectrum was finally selected for the prototype implementation.

B. Chamber Model

The detailed modeling of the chamber in an OWC device, from the fluid mechanics point of view, gives rise to complex mathematical models [18]–[20]. Nevertheless, the hardware implementation of the emulator imposes some limits because of RAM and cycle time constraints, so it is necessary to reach a compromise between the level of detail of the model and the capabilities of the hardware on which this model is running. As, from the point of view of electricity generation, a high degree of detail is not necessary, it was decided to use a simplified model.

The restrictions considered in the chamber model implemented in the microprocessor were as follows.

1) The air column inside the chamber is considered incompressible, so losses in the air have been neglected.
2) The height of the water surface inside the chamber is considered equal to the height reached by the wave. This assumption is reasonable when the wavelength of the incident ocean wave is much bigger than the dimensions of the water surface in motion inside the chamber.

Also, this means that the transfer function between the incident wave and the chamber oscillations, the memory effects related to wave radiation, and the effects of the force related to the pressure variation on the oscillating water mass are neglected. This makes the two systems, OWC and PTO, decoupled. As a consequence, the hydrodynamics inside the chamber is not fully described but, what it is more relevant from the electrical point of view, the electrical power delivered to the grid does not lose the multifrequency spectrum of the wave resource.

Thus, the air velocity in the duct of the turbine can be described by the following expression (see Table I in Appendix I for the nomenclature):

$$V_x = \left(\frac{A_c}{A_d}\right) \cdot \frac{\partial h_c}{\partial t}. \tag{1}$$

The chamber model implemented in the prototype is provided with a pressure relief valve. The function of this valve is to keep the torque coefficient of the turbine within the value given by the characteristic curve of the turbine just before stalling, when the value of the flow coefficient reaches or exceeds the stall point of the turbine [3], [21]. This model is calculated offline in the same PC where the wave profile is obtained.

C. Turbine Model

The shaft torque in the Wells type turbine has been mathematically modeled by the following equation [6], [22], [23] (see Table II in Appendix I for the nomenclature):

$$T_t = C_t \cdot K \cdot r_t \cdot \left[V_x^2 + (r_t \cdot \omega_t)^2\right]. \tag{2}$$

In this expression, the torque coefficient C_t depends on the characteristic curve of each particular turbine and it is a function of the air flow through the turbine by means of the flow coefficient Φ

$$\Phi = \frac{V_x}{r_t \cdot \omega_t}. \tag{3}$$

Fig. 2 shows, in solid line, the characteristic curve ($C_t - \Phi$) of the turbine model that has been represented in the prototype [6]. The efficiency curve is also shown in dashed line, where it can be noted that, from a certain value of Φ onwards, the turbine stalls and the efficiency falls sharply.

The torque calculated this way is the one that has to be reproduced in the prototype using a motor so that it will be the reference torque for the control algorithm.

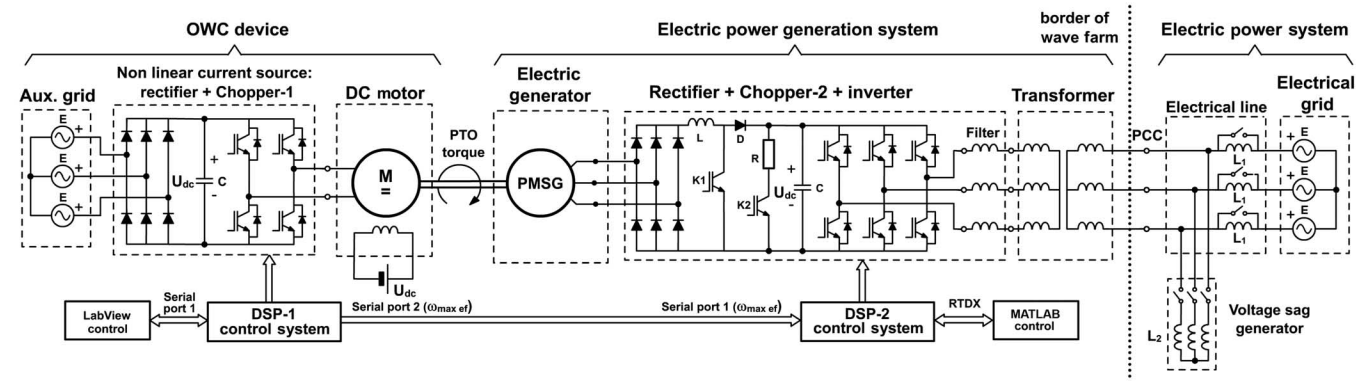

Fig. 3. *(Left)* Test rig used to carry out the experimental tests of the prototype (*right*) when connected to an electric power system.

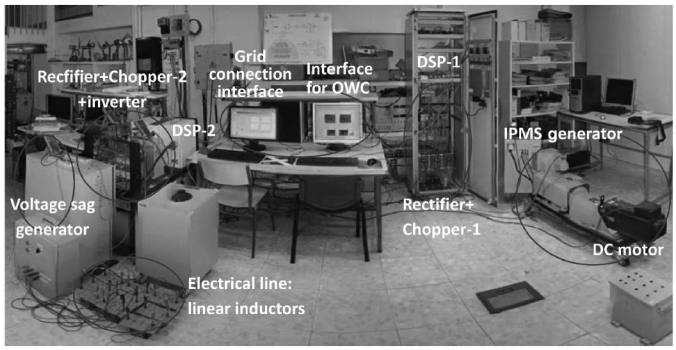

Fig. 4. Overview of the test rig.

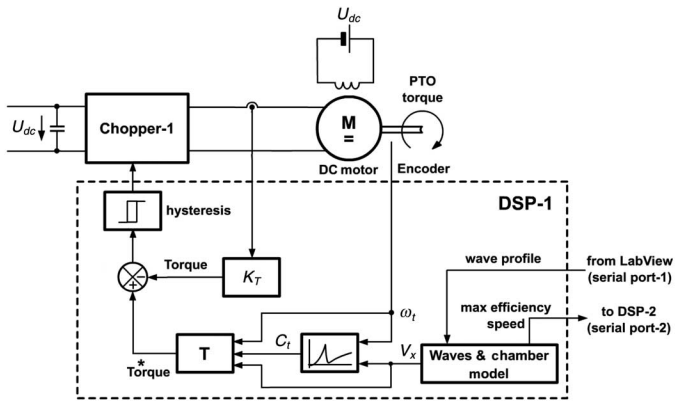

Fig. 5. Control system of the nonlinear current source implemented in the software of DSP-1 (dashed box) and used to control the dc motor by means of the Chopper-1.

III. Description of the Prototype

The prototype of the power plant is divided into two different systems: 1) the "OWC device" and the "electric power generation system." Fig. 3 shows the layout of both parts, along with an external electric power system to which the prototype is connected, and that absorbs the generated electrical power. A picture of the prototype is shown in Fig. 4.

A. OWC Device

As aforementioned, the prototype part that simulates the OWC device [24], [25] reproduces by means of the mathematical models described in Section II: the irregular wave profile, the chamber containing the OWC, and a Wells turbine.

Using the precalculated irregular wave profile, the control algorithm calculates, in each program cycle, the resulting turbine torque using the chamber and the Wells turbine models.

The torque generated in the turbine shaft is reproduced in real time using a separately excited dc motor. Although other options were considered (induction or permanent magnets), they were finally discarded because of the necessary complex control to accurately reproduce transient states of torque. In this type of dc motor, the torque depends directly on the armature current. Thus, to reproduce the dynamics of the turbine shaft produced by the oscillating movement of the water column, the control of the motor torque by means of this current must be very fast. Therefore, after evaluating several systems, a nonlinear current source [26] with a narrow hysteresis band and a 10-kHz switching frequency was chosen, avoiding the use of relatively slow P-I controllers in the current control loop.

Finally, the current source was carried out by implementing the control algorithm in a digital signal processor (DSP-1) and using a dc/dc converter (Chopper-1) (Figs. 3–5).

B. Electric Generation System

The second part of the prototype reproduces the whole electrical system of the OWC power plant and the electrical grid using real elements to scale (Figs. 3 and 4).

A permanent magnet synchronous generator (PMSG) connected to the turbine shaft was used to obtain electrical energy.

The grid connection was carried out using an uncontrolled three-phase rectifier and a dc/dc electronic converter (Chopper-2) and a three-phase inverter, both controlled by the DSP-2. Figs. 6 and 7 show the block diagrams of the control schemes programmed in DSP-2.

This configuration of the electric power generation system was selected because it is commonly used for the grid connection of small PMSG-based wind turbines. The reason is that it allows: on the one hand, the control of the electrical generator, and, on the other hand, the control of the active and reactive power delivered to the electrical grid.

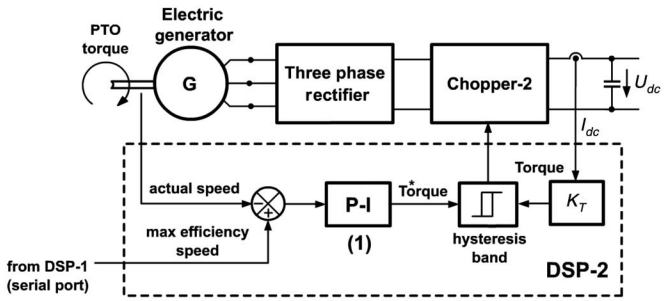

Fig. 6. Speed and torque control in the electric generator. The blocks inside the dashed box are implemented in the software of DSP-2.

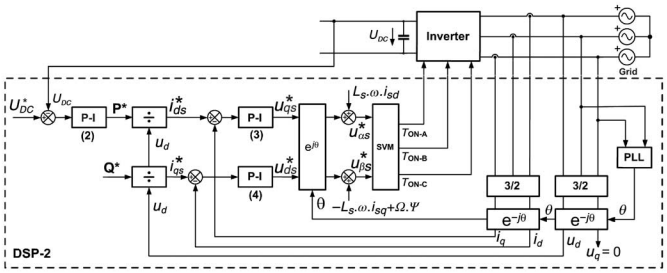

Fig. 7. Control system of the grid connection (DSP-2). The blocks inside the dashed box are implemented in the software of the DSP-2.

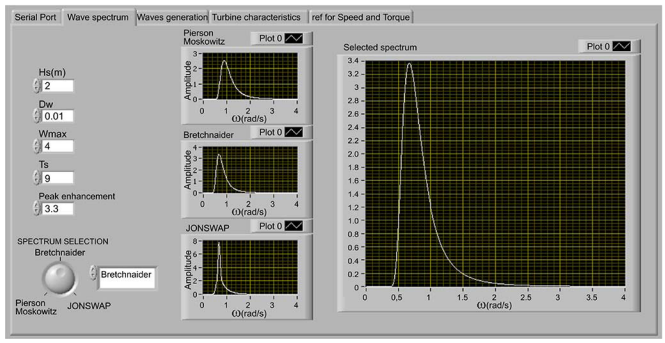

Fig. 8. Interface for setting the type of spectrum and the wave parameters.

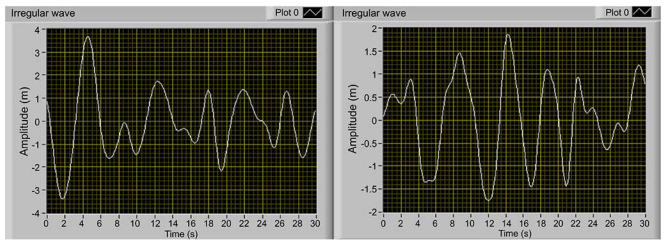

Fig. 9. Different wave profiles obtained with the same configuration.

The electric generator must generate the load torque to adjust the Wells turbine speed and to set it to the maximum efficiency point. To do this, the DSP-1 calculates, from the model of the turbine, the speed at which the Wells turbine shaft must turn and sends it periodically to the DSP-2 via the serial port (Figs. 3, 5, and 6).

The torque in the generator shaft can be controlled in an easy way using a rectifier and a dc–dc booster, because in this stage, after the noncontrolled rectifier, the voltage and current are dc so that no complex algorithms are needed such as space vector control.

The three-phase generator torque T_g, once the three-phase voltage is rectified, can be expressed through the output current of Chopper-2 I_{DC} as follows:

$$T_g \approx \frac{3 \cdot \sqrt{2}}{\pi} \cdot \left[\frac{E_g}{\omega_t}\right] \cdot I_{\mathrm{DC}} \approx K_T \cdot I_{\mathrm{DC}} \qquad (4)$$

where E_g is the electromotive force generated in the PMSG. Therefore, as it is shown in (4), the generator torque can be easily controlled by regulating the I_{DC} current in the booster.

The current control in Chopper-2 was performed using a nonlinear current source with a narrow hysteresis band and a 10-kHz switching frequency. The current reference is obtained from the torque reference calculated by the P-I regulator (Fig. 6). The proportional-integral-derivative (PID) regulators were avoided, as usual in these cases, because of the amplification of noise caused by the derivative part.

As usual in renewable energy generators, the control of the grid connection inverter has to be able to carry out independent active and reactive power control to meet the grid code requirements currently in use in most countries. For this reason, the control is carried out using spatial vectors and often includes a space vector modulator (SVM) like the implemented in the DSP-2 (Fig. 7).

This type of control systems are split into two subsystems composed of two nested loops. One of the subsystems controls the dc bus voltage so that if it raises, the P-I regulator increases the active power that the inverter delivers to the electrical grid whereas the other one regulates the reactive power. The P-Is in the inner (faster) loops have to be adjusted first, and then the outer (slower) ones. Next, the Park transformation is applied to the P-I outputs, then the SVM generates the pulses to control the inverter. The grid synchronization is accomplished using a phase-locked loop (PLL).

IV. Control Interfaces

Control software programming, visualization, and communication were carried out using three software tools: 1) LabVIEW; 2) Code Composer Studio; and 3) MATLAB.

Fig. 8 shows the interface developed to select the wave model (Pierson–Moskowitz, Bretschneider, JONSWAP) and configure the energy spectrum, $S(\omega)$.

Fig. 9 shows the result of two wave profiles obtained with exactly the same configuration (Pierson–Moskowitz), but using a different phase for each harmonic randomly generated in each simulation. The result is that, in each case, a different wave is generated, but both have the same energy content.

Another interface, programmed in MATLAB (left computer monitor in Fig. 4) allows the inverter to regulate the reactive power fed into the grid in real time and to record the active and reactive power values, current values, etc.

Finally, the two DSPs used were from the Texas Instruments TMS320F28335 model.

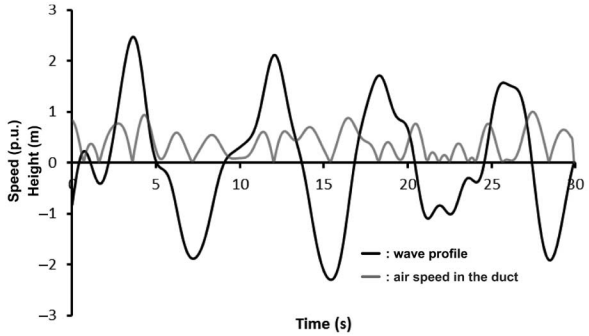

Fig. 10. Height of the free water surface of the wave (m) and air speed inside the turbine duct (expressed as absolute value in relation to its maximum).

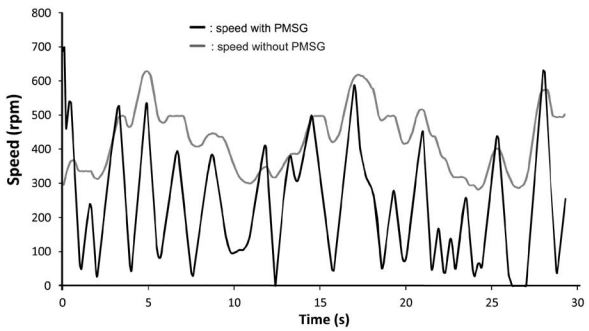

Fig. 11. Shaft speed of the turbine with the PMSG disconnected from the grid, and when the PMSG generates a load torque that leads to the turbine to work with maximum efficiency.

V. Experimental Results

This section compiles some experimental results obtained with the developed prototype. The aim is to show its performance under different scenarios, and to illustrate some of its capabilities and usefulness in the experimental validation of possible solutions to different electrical engineering problems posed in the operation of this kind of power generation technology.

A. Performance of the Prototype

To show the performance of the prototype, three different sets of tests are presented.

1) Test of the Chamber and Turbine Models: Once a wave model is selected and the wave profile is generated, two tests, with and without the grid connection system, were carried out. Fig. 10 shows the height of the free water surface of the wave and the air speed inside the duct of the turbine during the test. It can be seen that the air speed becomes zero each time the free water surface changes its movement direction.

Fig. 11 shows the shaft speed in both cases, with and without the electrical generator connected to the power system. It was found that, with the generator connected to the grid, a load torque is generated, which leads the turbine to the point of maximum efficiency speed. The speed difference observed in Fig. 11 is precisely due to the conversion of mechanical energy from the turbine shaft into electrical energy, which is fed into the grid.

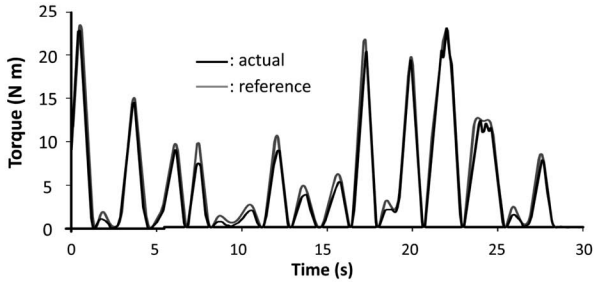

Fig. 12. Reference torque, calculated by the DSP-1, and actual torque measured in the PTO shaft.

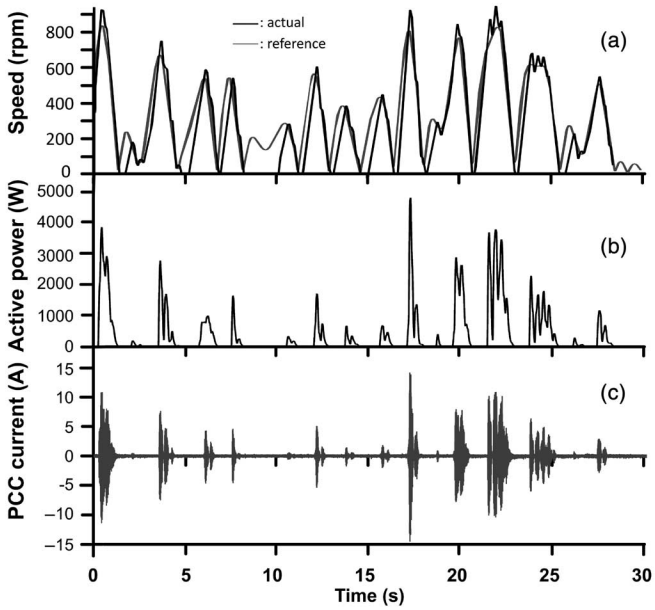

Fig. 13. (a) Reference speed for maximum efficiency and actual shaft speed. (b) Active power injected in the grid. (c) Electric current at the connection point.

In particular, most of the power extraction obtained does not occur at the moment of increasing speed but during decreasing speed. Indeed, on the rise, the generator only limits the turbine speed following the point of maximum efficiency. However, it is from the maximum speed points when the torque created by the generator slows down the turbine speed, thus producing most of the electromechanical energy conversion.

2) Tests of the Whole Power Plant: In the following test, the behavior of the power plant from the electrical engineering point of view was studied, using the dimensions of Table III.

Fig. 12 shows the actual and the reference torque calculated in the DSP-1 from the turbine model. The dc motor torque is controlled with a nonlinear current source implemented in the chopper control algorithm. In this way, the large torque variations that appear in the PTO shaft due to the oscillations of the water column inside the chamber are reproduced.

Fig. 13(a) shows the maximum efficiency speed, calculated on the DSP-1 and sent as reference speed to the DSP-2, as well as the actual PTO speed during the test. It was found that the load torque presented by the PMSG leads to the turbine operating at the maximum efficiency speed.

Concerning the operation of the electrical part of the power plant, Fig. 13(b) shows the active power profile fed into the grid.

It can be seen that there are large low-frequency fluctuations (a peak-to-average power ratio of 13.9) that are very difficult to filter, which is the main problem in this type of power plant, both from the component fatigue and the electrical grid points of view.

A number of solutions for mitigating such fluctuations can be applied. For example, at the machine level, the inertia can be increased with a flywheel, although it leads to a reduction of efficiency because of the slower transient response, or the flux coefficient target can be changed within a range around the optimum. These solutions should be a compromise between the limitation of power fluctuations and the reduction of efficiency. At the grid level, electrical energy storage solutions, e.g., with ultracapacitors, can be applied. These solutions smooth the fluctuations of the power injected into the grid, with little loss of efficiency, but they do not mitigate the fluctuations at the machine level.

Finally, Fig. 13(c) depicts the current fed into one of the phases of the electrical grid during the test.

Note that there is a very precise speed tracking during the deceleration intervals because the control on the electric generator allows a fast load torque regulation. However, during the acceleration intervals, the speed tracking cannot be so fast because the accelerating torque only can be obtained from the turbine since the generator cannot be used as a motor because of the uncontrolled rectifier. Even in the case of using a bidirectional converter, it still would not be appropriate because it would involve power consumption from the grid.

Nevertheless, if this were allowed the speed tracking during the acceleration process would be equally precise and the whole system would work more efficiently. This situation becomes much clearer when the Wells turbine torque is low and coincident with zero speed. In these conditions, the torque may be too low to compensate the friction torque during short time intervals, e.g., around $t = 8$ s in Fig. 13(a).

3) Test With a Lower Wave Spectrum: In this test, the chamber and turbine dimensions of the first test, Table III, were used again, but the significant wave height H_S was reduced from 2 to 0.8 m to represent a less energetic wave. The remaining variables were kept at the default values as shown in Table III. Now, the resulting torque is lower than the one in the first test, although the dimensions of the chamber and the turbine are the same (Fig. 14). It is a direct consequence of the lower wave energy content.

Fig. 15(b) shows how, with a reduced wave energy spectrum, the power delivered to the grid decreases. While in the previous test, the active power reaches values of around 4.7 kW [Fig. 13(b)], for this test, a power plant with the same dimensions but with reduced spectrum conditions feeds just about 1.1 kW into the grid.

B. Using the Prototype in Electrical Engineering Research

The previous tests show how the slow motion of the water and the variability in the wave profile result in great variability in the power and the current fed into the electrical grid. This kind of fluctuations affects the power quality and causes problems in the power system operation and control. To improve the

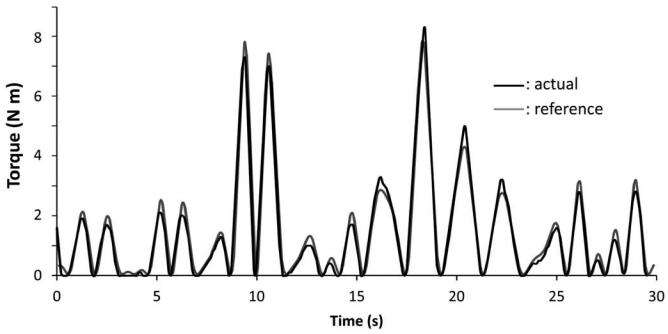

Fig. 14. Reference torque, calculated by the DSP-1, and actual torque in the PTO shaft.

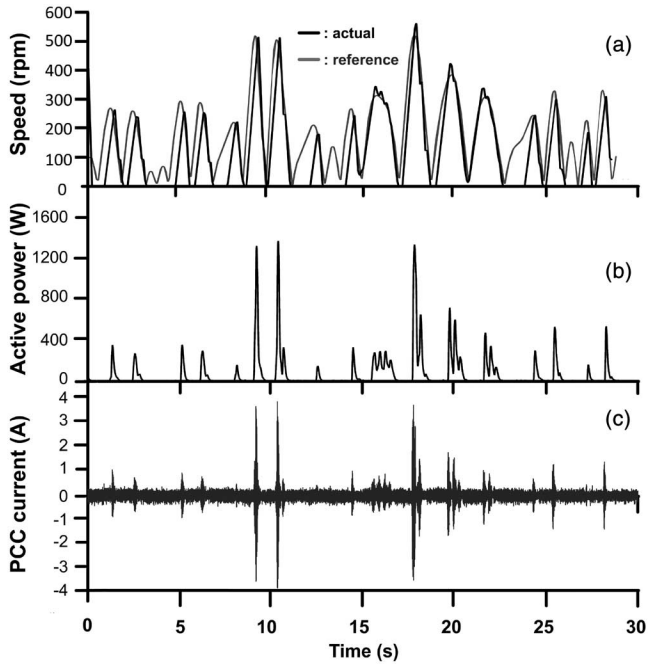

Fig. 15. (a) Reference speed for maximum efficiency and actual shaft speed. (b) Active power injected in the grid. (c) Electric current at the connection point.

penetration of this kind of energy into power systems, it is necessary to filter or absorb such fluctuations, what is a challenge due to their amplitude and very low frequency. In the case of onshore OWC extractors, it is not possible to optimize the location of each individual chamber in the plant to shift the arrival of wave peaks to have a smoother global power production of the plant, as it is the case with other wave energy converters, like point absorbers. The developed prototype can be used to test different solutions to this problem at a laboratory scale, e.g., the use of flywheels, batteries, fuel cells, and ultracapacitors.

An interesting field in which the use of the system is related to the investigation of the ability of the system to comply with the connection requirements imposed by transmission operators, particularly exigent in countries with a high degree of renewable energy penetration. As an example, the developed prototype has been used to test its low-voltage ride-through capability according to the Spanish grid code PO 12.3 [27].

To verify the behavior of an OWC power plant during voltage dips, a laboratory experiment was performed using the test rig

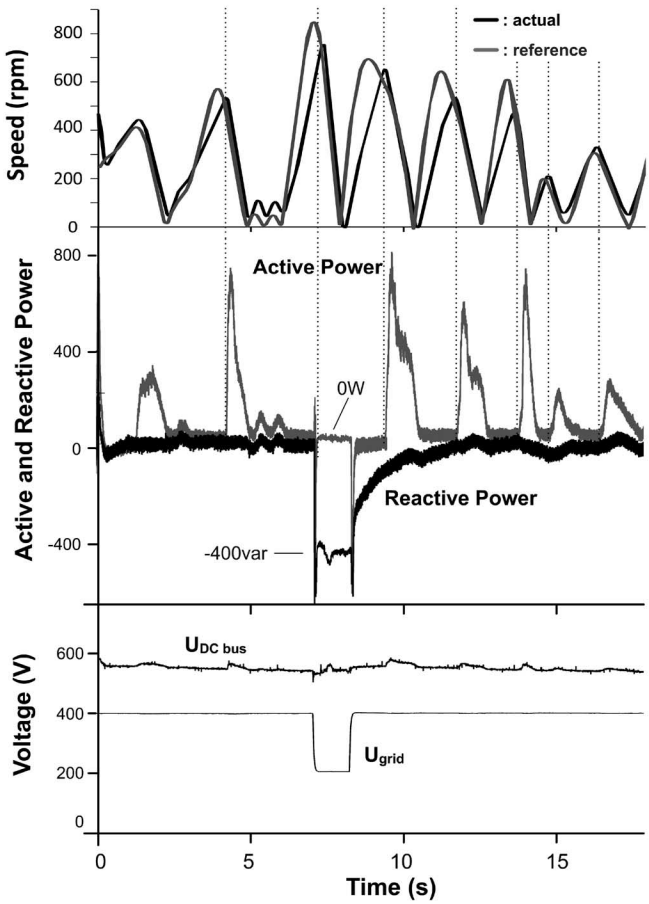

Fig. 16. Reference speed and actual shaft speed during the voltage dip.

of Fig. 3, as described previously. Then, a voltage sag test was carried out to verify the degree of compliance with the grid code during a three-phase fault (Fig. 16). In the case of unbalanced faults, similar tests can be carried out by decomposing the grid voltage in its positive and negative sequences and then compensating both sequences separately. This kind of test is usual in all the renewable generators connected to the grid and mandatory in most of the cases.

During the test, a voltage dip with a 50% residual value was generated, just before the instant when maximum speed was reached ($t = 7$ s). In normal operating conditions, without the voltage dip, the torque generated by the electric generator reduces the speed of the turbine shaft by feeding electric power into the grid. However, in this case, it is not possible due to the low grid voltage, because it is necessary to comply with the grid code that sets the relationship between active and reactive powers in this kind of situations. The effect of the incoming power in the dc bus is to increase the U_{DC} voltage. Although there are several methods, one of the most common renewable generators control is to use a controlled dissipation of the active power delivered by the generator. To carry it out, a resistor R and the switching of an insulated-gate bipolar transistor (IGBT), K2 in Fig. 3, were used to keep constant the value of U_{DC} .

The criterion for sizing R is based on the worst-case scenario, in which the generator is producing maximum power and there is a zero-volts voltage sag that makes electric power delivery to the grid impossible.

As seen in Fig. 16, the PTO shaft speed was not affected by the voltage dip due to the load torque created by the power dissipation in the resistor.

The generation system remained connected during the voltage dip and it delivered a large amount of reactive power, Fig. 16, fulfilling the restriction $I_{\mathrm{reactive}}/I_{\mathrm{total}} > 0.9$ imposed by the Spanish Grid Code. A small perturbation in the reactive power appears when the dissipation of active power begins, just after the maximum speed. Once the PI controllers have adjusted the power, the perturbation disappears.

Also, it can be seen that there was no active power fed into the grid during the voltage dip because all the input power from the Wells turbine emulator and the electric generator was dissipated in R. Also, after the voltage dip, the active power remains during a certain interval at $P = 0$ since, in this moment, the turbine speed is increasing, so no power extraction is carried out.

VI. Conclusion

A prototype whose main purpose is to study an OWC power plant from the point of view of the power fed into the electrical grid has been presented. The system has two important features. 1) It can reproduce irregular waves, which are characterized by several statistical models of real waves corresponding to specific areas of the ocean rather than traditional models of regular waves (sinusoidal) to analyze the electrical power injected into the grid. 2) A PMSG has been used in the tests, since these machines are the trend for marine applications. The test rig also allows to test new solutions to mitigate the large low-frequency oscillations characteristic of the generated active power.

To demonstrate the performance of the prototype under different operating conditions, several tests have been carried out for different types of real waves and power plant sizes. In all the cases, results congruent with the setup of the prototype were obtained, including the large low frequency variations in the generated power.

The usefulness of the prototype in the investigation of possible solutions to improve the operation of this kind of power generation technology has been illustrated with a study on the ability of the OWC power plants to comply with the connection requirements imposed by the Spanish Grid Code. This study has shown that the low inertia of the Wells turbine can cause a dangerous acceleration if neither dissipation systems nor storage systems are used for the electrical energy generated during the fault.

Appendix I: Nomenclature

TABLE I
Chamber Model

V_x	Air speed in the duct (m/s)
h_c	Height of the free water surface inside the chamber (m)
A_c	Chamber cross section (m^2)
A_d	Duct cross section (m^2)
r_d	Duct radius (m)

TABLE II
TURBINE MODEL

T_t	Shaft torque (N m)	r_t	Turbine radius (m)
ϕ	Flow coefficient (non dimensional)	V_x	Air speed in duct (m/s)
C_t	Torque coefficient (non dimensional)	ω_t	Angular velocity of rotor system (rad/s)
K	Constant of the turbine (kg/m)		

TABLE III
DEFAULT VALUES

Model: Pierson–Moskowitz	Maximum C_t before stall	for $\phi = 0.311$
$A_c = 15$ m^2	Air density	$\rho = 1.2$ kg/m^3
$r_d = 0.5$ m	Height of the blades	$b = 0.0723$ m
$r_t = 0.5$ m	Blade chord length	$l = 0.059$ m
Maximum efficiency flux $\phi_{\max ef} = 0.17$ m	Number of turbine blades	$n = 8$

APPENDIX II: RATED VALUES AND CONSTANTS OF SEVERAL COMPONENTS USED IN THE TEST RIG

TABLE IV
MOTOR AND GENERATOR

DC motor		PMS generator	
P_N	7.8 kW	P_N	8.7 kW
U_N	400 V	U_N	400 V
n_N	1090 rpm	n_N	1000 rpm
K_T	3.1	K_T	6.5

TABLE V
RATED VALUES OF THE TRANSFORMER AND THE INDUCTORS

Transformer for grid connection		Inductor in the grid connection	
S_N	10 kVA	L	8 mH
U_N	400/230 V	Inductor in Chopper-2	
Capacitor in dc bus		L	100 mH
C	2350 μF	R	18.4 Ω

TABLE VI
CONSTANTS OF THE P-I REGULATORS USED IN THE ELECTRIC POWER GENERATION SYSTEM

P-I: $U(s) = K_p \cdot \left(\frac{s+a}{s}\right) \cdot I(s)$

	P-I (1)	P-I (2)	P-I (3)	P-I (4)
K_p	0.02	0.5	2.25	4.5
a	0.01	0.2	0.02	4.5

REFERENCES

[1] B. Drew, A. R. Plummer, and M. N. Sahinkaya, "A review of wave energy converter technology," in *Proc. Inst. Mech. Eng. A: J. Power Energy*, 2009, pp. 223–887.

[2] F. Neumann, A. Brito-Melo, E. Didier, and A. Sarmento, "Pico OWC recovery project: Recent activities and performance data," presented at the Eur. Wave Tidal Energy Conf., Porto, Portugal, 2007.

[3] A. F. O. Falcao and P. A. P. Justino, "OWC wave energy devices with air flow control," *Ocean Eng.*, vol. 26, no. 12, pp. 1275–1295, 1999.

[4] F. Paparella, K. Monk, V. Winands, M. F. P. Lopes, D. Conley, and J. V. Ringwood, "Up-wave and autoregressive methods for short-term wave forecasting for an oscillating water column," *IEEE Trans. Sustain. Energy*, vol. 6, no. 1, pp. 171–178, Jan. 2015.

[5] D. Somayajula and M. L. Crow, "An ultracapacitor integrated power conditioner for intermittency smoothing and improving power quality of distribution grid," *IEEE Trans. Sustain. Energy*, vol. 5, no. 4, pp. 1145–1155, Jul. 29, 2014.

[6] M. Amundarain, M. Alberdi, A. J. Garrido, and I. Garrido, "Modeling and 6 simulation of wave energy generation plants: Output power control," *IEEE Trans. Ind. Electron.*, vol. 58, no. 1, pp. 105–117, Jan. 2011.

[7] D. B. Murray, J. G. Hayes, D. L. O'Sullivan, and M. G. Egan, "Supercapacitor testing for power smoothing in a variable speed offshore wave energy converter," *IEEE J. Ocean. Eng.*, vol. 37, no. 2, pp. 301–308, Apr. 2012.

[8] *Recommended Practice. DET NORSKE VERITAS (DNV) DNV-RP-C205. Environmental Conditions and Environmental Loads*, Oct. 2010.

[9] W. J. Pierson and L. Moskowitz, "A proposed spectral form for fully developed wind seas based on the similarity theory of S.A. Kitaigorodskii," *J. Geophys. Res.*, vol. 69, pp. 5181–5190, 1964.

[10] L. Moskowitz, W. J. Pierson, and E. Mehr, "Wave spectra estimated from wave records obtained by the OWS Weather Explorer and the OWS Weather Reporter," Parts 1, 2 and 3, U. S. Naval Oceanographic Office, New York Univ., Tech. Rep. 63-5, 1962.

[11] G. J. Komen and K. Hasselmann, "On the existence of a fully developed wind-sea spectrum," *J. Phys. Oceanogr.*, vol. 14, no. 8, pp. 1271–1285, Aug. 1984.

[12] K. Hasselmann *et al.*, "Measurements of wind-wave growth and swell decay during the joint North Sea Wave Project (JONSWAP)," *Dtsch. Hydrogr. Z. Suppl.*, vol. 12, no. A8, pp. 31–55, 1973.

[13] D. E. Hasselmann, M. Dunckel, and J. A. Ewing, "Directional wave spectra observed during JONSWAP 1973," *J. Phys. Ocean.*, vol. 11, pp. 718–728, 1980.

[14] Y. Goda, *Random Seas and Design of Maritime Structures*, 3rd ed. Singapore: World Scientific Publishing Co., 2010. ISBN: 978-981-4282-39-0.

[15] Y. Goda, "Analysis of wave grouping and spectra of long-travelled swell," *Rep. Port Harbour Res. Inst.*, vol. 22, no. 1, pp. 1–40, 1983.

[16] E. Bouws, H. Günther, W. Rosenthal, and C. L. Vincent, "Similarity of the wind wave spectrum in finite depth water: 1. Spectral form," *J. Geophys. Res.*, vol. 90, no. C1, pp. 975–986, 1985.

[17] W. Mitsuyasu, "Development of spectra of wind and waves (2)," in *Proc. 17th Coastal Eng. Conf.*, 1970, pp. 1–7.

[18] J. W. Weber and G. P. Thomas, "An investigation into the importance of the air chamber design of an oscillating water column wave energy device," in *Proc. 11th Int. Offshore Polar Eng. Conf.*, Stavanger, Norway, 2001, pp. 17–22.

[19] A. Falcao, J. C. C. Henriques, and J. J. Candido, "Dynamic and optimization of the OWC spar buoy wave energy converter," *Renew. Energy*, vol. 48, pp. 369–381, 2012.

[20] W. Sheng, R. Alcorn, and A. Lewis, "Assessment of primary wave energy conversions of oscillating water columns. I. Hydrodynamic analysis," *J. Renew. Sustain. Eng.*, vol. 6, p. 053113, 2014.

[21] A. F. O. Falcao, L. C. Vieira, P. A. P. Justino, and J. Anfre, "By-pass air-valve control of an OWC wave power plant," *J. Offshore Mech. Arct. Eng.*, vol. 125, no. 3, pp. 205–210, 2003.

[22] M. Inoue, K. Kaneko, T. Setoguchi, and T. Saruwatari, "Studies on the Wells turbine for wave power generator (turbine characteristics and design parameter for irregular wave)," *JSME Int. J.*, vol. 31, no. 4, pp. 676–682, 1988.

[23] S. Raghunathan, "The Wells air turbine for wave energy conversion," *Prog. Aerosp. Sci.*, vol. 31, no. 4, pp. 335–386, 1995.

[24] M. Alberdi, M. Amundarain, A. J. Garrido, I. Garrido, O. Casquero, and M. De la Sen, "Complementary control of oscillating water column-based wave energy conversion plants to improve the instantaneous power output," *IEEE Trans. Energy Convers.*, vol. 26, no. 4, pp. 1021–1032, Dec. 2011.

[25] W. K. Tease, J. Lees, and A. Hall, "Advances in oscillating water column air turbine development," presented at the Eur. Wave Tidal Energy Conf., Porto, Portugal, 2007.

[26] S. Buso, L. Malesani, and P. Mattavelli, "Comparison of current control techniques for active filter applications," *IEEE Trans. Ind. Electron.*, vol. 45, no. 5, pp. 722–729, 1998.

[27] M. Alberdi, M. Amundarain, A. J. Garrido, I. Garrido, and F. J. Maseda, "Fault-ride-through capability of oscillating-water-column-based wave-power-generation plants equipped with doubly fed induction generator and airflow control," *IEEE Trans. Ind. Electron.*, vol. 58, no. 5, pp. 1501–1517, May 2011.

Dionisio Ramirez (M'07–SM'15) was born in Spain, in 1966. He received the M.S. degree in industrial engineering and the Ph.D. degree in electrical engineering from the Universidad Politecnica de Madrid (UPM), Spain, in 1997 and 2003, respectively.

He is an Associate Professor with the Department of Electrical Engineering with the UPM. His research interests include electric control of renewable energy and control systems based in DSPs.

Juan Pablo Bartolome received the M.S. degree in electrical engineering from the Universidad Simon Bolivar, Caracas, Venezuela, in 2008 and the M.S. degree in electrical engineering from the Universidad Politecnica de Madrid, Madrid, Spain, in 2011.

Currently he is working in an electrical company in Caracas, Venezuela.

Sergio Martinez (M'02) was born in Spain, in 1969. He received the M.S. degree in industrial engineering and the Ph.D. degree in electrical engineering from the Universidad Politecnica de Madrid (UPM), Madrid, Spain, in 1993 and 2001, respectively.

He is an Associate Professor with the Department of Electrical Engineering, UPM. His research interests include electrical generation from renewable energy and electrical metrology.

Luis Carlos Herrero (M'11) received the B.Sc. (Hons.), M.S.E.E., and Ph.D. degrees in electronics engineering from the University of Valladolid, Valladolid, Spain, in 1986, 1992, and 2005, respectively.

Since 1994, he has been an Associate Professor with the Electronic Technology Department, University of Valladolid, involved in the development and design of analog and digital power electronics systems. He teaches courses in power electronics. His main research areas are direct ac/ac converters, new converter topologies, and power electronics conditioners with PWM sliding inverters for ac motors controllers and photovoltaic systems. Currently, he is involved in research and development of industrial projects in the areas of photovoltaic (CC/CA) and wind generators (CA/CA).

Marcos Blanco received the M.S. degree in electrical engineering from the Universidad Politecnica de Madrid, Madrid, Spain, in 2008.

His research interests include power electronic converters, DSP-based control, ocean wave energy generation, and electrical drives control.